BiomSHARP: **Biom**ass **S**uper-resolution for **H**igh **Accur**acy **P**rediction

Laia Albors, Javier Marcello, *Senior Member, IEEE,* and Ferran Marques, *Senior Member, IEEE*

***Abstract*—Accurate estimation of above-ground biomass (AGB) is essential to understanding carbon stocks and flows, monitoring forest health, assessing biodiversity, and tracking ecological disturbances, which together help to inform climate policies. Imminent global satellite biomass missions (such as ESA's BIOMASS and NASA-ISRO's NISAR satellites) will offer valuable environmental monitoring, but their low spatial resolution limits their application in detailed local assessments. In this study, we present BiomSHARP (Biomass Super-resolution for High Accuracy Prediction), a deep learning (DL) model developed to enhance coarse-resolution biomass maps by fusing them with high-resolution multispectral data from sensors such as Sentinel-2 or Landsat. BiomSHARP achieves 25-meter biomass predictions—four times the spatial resolution of the input—bridging the gap between global-scale monitoring and local-scale applications. In a first set of experiments, conducted in a local area in Europe, we demonstrate that BiomSHARP outperforms both traditional interpolation methods and state-of-the-art DL interpolation and prediction approaches for high-resolution AGB estimation across all evaluated metrics (MAE, MSE, RMSE, PSNR and SSIM), while using a comparable/lower number of parameters. Moreover, the model exhibits strong global-scale generalization, as demonstrated by its ability to accurately estimate biomass across diverse climatic regions despite being trained on a limited subset of data. Furthermore, the model presents strong temporal generalization, achieving improved performance in estimating AGB from 2020 data even when trained solely on 2010 data. We also analyze the impact of different combinations of spectral bands on biomass estimation, identifying optimal subsets that reduce redundancy and improve computational efficiency. BiomSHARP represents a promising approach to advance global environmental assessments and support improved climate strategies. The code and models are publicly available at https://github.com/laiaalbors/biomsharp.**

***Index Terms*—BiomSHARP, Above-ground biomass, Guided biomass super-resolution, Deep learning, Remote sensing, Multispectral imagery, Satellite biomass estimation, Climate monitoring.**

I. Introduction

THE increasing effects of climate change highlight the critical need to deepen our understanding of global ecosystems. A key element in this understanding is the accurate estimation of above-ground biomass (AGB), essential for modeling carbon stocks and flows, monitoring forest health, assessing biodiversity, and tracking ecological disturbances such as fires or storms—which in turn shape effective climate policies [1]. Time-consuming, cost-effective, and non-invasive methods for global biomass estimation are indispensable, offering vital data while preserving the studied ecosystems. The recent development of satellite technologies dedicated to estimating AGB reflects a global consensus on the importance of these estimates. For example, the planned launches in 2025 of ESA's BIOMASS satellite [2] and NASA-ISRO's NISAR mission [3] mark major progress towards regular, non-destructive monitoring of global biomass—including in hard-to-reach areas. This is crucial for both understanding and combating the effects of climate change.

However, while these satellite missions will provide the global overview necessary for broad environmental assessments, they will not deliver the detailed data achieved with local studies. This is due to their limited resolutions—200 meters for the BIOMASS satellite [2] and 100 meters for the NISAR mission [3]. Detailed data is essential for designing specific, local-level actions and policies. These local assessments, critical for the development of particular interventions, are notably expensive, labor-intensive, and logistically complex, particularly in remote areas where accessibility poses significant challenges.

To address these limitations, this paper proposes BiomSHARP, an innovative approach using deep learning (DL) to merge low-resolution biomass data, such as that of BIOMASS or NISAR upcoming satellite missions, with high-resolution multispectral data from satellite sensors such as Sentinel-2 or Landsat. This combination aims to produce high-resolution biomass maps capable of providing detailed insights for any region of the world. By leveraging the strengths of both satellite systems, our method offers a promising solution to bridge the gap between global monitoring capabilities and local application needs, enabling detailed environmental assessments on a global scale.

Hence, the primary objective of this work is to develop a DL tool that enhances the resolution of low-resolution AGB maps, specifically transforming 100-meter resolution data into 25-meter resolution data.

This paper makes three key contributions: (1) we introduce BiomSHARP, a novel deep learning architecture for guided super-resolution of AGB maps that outperforms current state-of-the-art models across all tested metrics; (2) we conduct a detailed analysis of multispectral bands to identify the optimal subset that minimizes redundancy while maintaining performance; and (3) we release publicly available pretrained checkpoints for both Landsat-5 and Sentinel-2 data that have demonstrated robust spatial and temporal generalization in improving the resolution of AGB maps. These checkpoints include global and climate-specific models, allowing practi-

Laia Albors and Ferran Marqués are with Signal Theory and Communications Department, Universitat Politècnica de Catalunya, BarcelonaTech, 08034 Barcelona, Spain (e-mail: laia.albors@upc.edu, ferran.marques@upc.edu).

Javier Marcello is with Instituto de Oceanografía y Cambio Global, IOCAG, Unidad Asociada ULPGC-CSIC, 35017 Las Palmas de Gran Canaria, Spain (e-mail: javier.marcello@ulpgc.es).

tioners to choose the most suitable variant for their region or application.

The structure of this paper is as follows: after this introduction, Section II reviews relevant literature, focusing on methodologies for AGB estimation using remote sensing and on recent advancements in super-resolution techniques. Section III details the data used, including the datasets, preprocessing techniques, and regions of study. Section IV describes the methodologies employed in our study, including the comparison baselines and the characteristics of the proposed DL model. Section V presents four key experiments—comparing BiomSHARP with state-of-the-art methods, assessing the impact of reducing band redundancy, testing global-scale generalization, and evaluating temporal generalization—which together demonstrate the superior performance of BiomSHARP with respect to the baselines. Finally, Section VI concludes the paper, summarizing the key contributions of our work, stating the limitations of this study, and suggesting potential directions for future research.

II. Related Work

This section reviews prior research relevant to our study, focusing on two key areas: the estimation of AGB using remote sensing data and advancements in image super-resolution techniques. The first part highlights traditional and deep learning-based approaches for biomass prediction, emphasizing their strengths and limitations in local and global contexts. The second part analyzes image super-resolution methodologies, including guided super-resolution, and their applicability to enhancing biomass data resolution, framing the state-of-the-art techniques that inspire our proposed model.

A. Above-Ground Biomass Estimation from Remote Sensing Data

1) Local Estimations: Numerous studies have investigated the prediction of AGB using remote sensing (RS) data. The majority of these studies use optical satellite imagery from platforms like Sentinel-2 and Landsat [4]–[8]. Other works have employed optical data collected by Unmanned Aerial Vehicles (UAVs) [9], whereas some have explored the use of RADAR data from sources such as Sentinel-1, ALOS, and Gaofen-3 [7], [10].

Within these studies, traditional Machine Learning (ML) techniques are most commonly used, typically relying on manual feature extraction from the RS data [4]–[6], [10]. However, recent studies have proposed more advanced DL models that do not require prior feature extraction, working directly on raw data [7]–[9]. For instance, [7] compares traditional machine learning methods like Random Forest (RF) [11] with deep learning models such as CNN [12] and CNN-LSTM [13], and it concludes that deep learning approaches, particularly CNN-LSTM, perform better in predicting AGB when using multispectral and SAR data, due to their capacity to handle complex relationships and to extract high-dimensional features from these types of RS data.

While these studies provide valuable information for local actions by offering resolutions up to 2.5 meters, they lack the broader, global insights essential for understanding the global carbon cycle and informing climate mitigation policies. This limitation arises because these studies have been conducted in relatively small areas, at most a few thousand square kilometers.

2) Global Estimations: In parallel, a different approach has been proposed that focuses on improving global understanding by creating worldwide biomass maps. Earlier versions of these maps often had low spatial resolutions, typically between 500 and 1,000 meters [14]–[16]. While these low-resolution maps provided essential data for global assessments, their utility for localized applications was limited. Moreover, with the imminent launch of the BIOMASS and NISAR satellites—set to provide worldwide estimations of AGB at 200 and 100 meters resolution, respectively—these maps will become outdated.

More recent studies have produced higher-resolution biomass maps (up to 30 meters) targeting specific regions like tropical forests [17], global mangrove forests [18], and even encompassing all global forest types [19]. These advancements have significantly extended the applicability of biomass maps for regional and local analyses, offering more actionable data for forest management and conservation while maintaining their usefulness for global assessments.

However, producing these high-resolution maps involves complex methodologies that rely on multiple data sources and intricate processes. Generally, they require region-specific allometric equations (mathematical models tailored to specific tree species or forest types) to estimate biomass from measurable tree parameters. LiDAR (Light Detection and Ranging) data, captured by UAVs or satellites, is also utilized to compute the ground truth AGB in conjunction with these allometric equations. Classic machine learning models, such as RF, are then trained to link biomass with other satellite-derived data (including imagery, elevation, and climate variables) to obtain continuous biomass maps. Despite their utility, these methods are data-intensive and computationally complex—factors that limit both their scalability and accessibility.

B. Image Super-Resolution

Considering the previously commented launch of biomass satellites (which will provide worldwide low-resolution AGB data), as well as the availability of a dataset with global biomass estimations at a higher resolution [20]–[28], we propose the novel application of image super-resolution techniques for global high-resolution biomass estimation. Super-resolution (SR) refers to the task of generating high-resolution images from one or more low-resolution captures of the same scene [29]. In our case, we address single-image super-resolution. Conventional linear interpolation schemes, such as bilinear and bicubic interpolation, have been widely used to generate high-resolution images from low-resolution versions due to their computational simplicity. However, these methods fall short in capturing high frequency data, often resulting in blurred edges and noticeable artifacts in the interpolated images [30]. To address these issues, many super-resolution algorithms have been proposed over the years [31]. Among them are reconstruction-based methods, which iteratively enhance resolution using prior image statistics. Another group of

TABLE I
OVERVIEW OF THE DATA USED IN EACH EXPERIMENT, INCLUDING THE SECTION WHERE EACH EXPERIMENT IS DISCUSSED, THE REGION OF STUDY, THE YEARS OF THE ABOVE-GROUND BIOMASS (AGB) AND MULTISPECTRAL (MS) DATA USED FOR TRAINING AND VALIDATION, AND THE MULTISPECTRAL BANDS CONSIDERED. AGB DATASETS INCLUDE HIGH-RESOLUTION SOURCES (GLOBBIOMASS, FORMS) AND LOW-RESOLUTION SOURCES (ESA BIOMASS CLIMATE CHANGE INITIATIVE). MULTISPECTRAL DATA COME FROM LANDSAT-5 LEVEL-2, COLLECTION 2, TIER 1 PRODUCT (L5) AND SENTINEL-2 LEVEL-2 PRODUCT (S2).

Section	Experiment	Region of Study	Year of the Data				Multispectral Bands
			Training		Validation		
			AGB	MS	AGB	MS	
V-A	SOTA Comparison	AoI	2010 (Glob/ESA)	2010 (L5) 2017 (S2)	2010 (Glob/ESA)	2010 (L5) 2017 (S2)	All
V-B	Band Redundancy	AoI	2010 (Glob/ESA)	2010 (L5) 2017 (S2)	2010 (Glob/ESA)	2010 (L5) 2017 (S2)	Different combinations
V-C	Global Generalization	Global	2010 (Glob/ESA)	2009-2011 (L5) 2017-2019 (S2)	2010 (Glob/ESA)	2009-2011 (L5) 2017-2019 (S2)	3, 4, 7 (L5) 4, 8, 12 (S2)
V-D	Temporal Generalization	AoI / France	2010 (Glob/ESA)	2017 (S2)	2020 (FORMS/ESA)	2020 (S2)	4, 8, 12 (S2)

methods includes example-based super-resolution techniques, which use a dictionary of high-resolution patches to guide finer detail inference in low-resolution images [31].

Despite these advancements, traditional super-resolution methods still face challenges in effectively capturing complex image structures and generalizing across diverse datasets. These limitations have driven the exploration of more sophisticated approaches that can learn intricate mappings and adapt to varying data characteristics, such as DL-based interpolation methods. In particular, SRCNN [32] was the first method to introduce deep CNNs to the image super-resolution task, obtaining superior performance over traditional super-resolution methods. After this work, many other DL models [4], [33]–[42] were proposed to further improve this field. Among these, we need to highlight the HAT (Hierarchical Attention Transformer) model, introduced in [41] and further developed in [42], which represents a significant advancement in super-resolution technology. HAT innovatively combines self-attention, channel attention, and overlapping cross-attention to address key limitations of Transformer-based SR models. These include limited receptive field, insufficient pixel utilization, and blocking artifacts. As a result, HAT achieves superior accuracy and visual quality.

1) Guided Super-Resolution: Within the realm of image super-resolution, guided super-resolution represents a specialized subtask, which uses high-resolution (HR) images to help enhance low-resolution (LR) data. This technique has already been used to enhance the resolution of various types of data, such as depth maps [43]–[46], thermal images [47]–[49], hyperspectral images [50]–[52], feature maps [53], and even other RGB images [54], using HR RGB images as guidance. However, to the best of our knowledge, this paper is the first to apply this technique for enhancing the resolution of biomass data.

Among the various guided super-resolution tasks, depth map super-resolution shares several characteristics with biomass data enhancement. Both depth and biomass rasters are typically single-channel and contain values that correspond to physical quantities. Additionally, they often exhibit clear structural boundaries aligned with physical objects, unlike thermal or feature maps, where values may be more abstract or spatially diffuse. In this context, SGNet [43] improves depth map resolution by leveraging gradient and frequency information to preserve structural details and high-frequency components. These properties are also desirable for biomass super-resolution, where edge preservation and accurate reconstruction of physical values are critical.

Recent research has explored guided super-resolution using diffusion models, particularly for depth maps. For instance, the study in [55] introduces a diffusion model within the latent space to generate guidance for depth map super-resolution. Analogously, [56] presents a similar approach, focusing on efficient feature fusion and reconstruction using diffusion models. However, SGNet, which uses non-diffusion models to improve depth map resolution, outperforms these proposals. For this reason, we have not included diffusion-model-based approaches in this study.

Inspired by these state-of-the-art methodologies, our proposed approach aims to generate high-resolution biomass maps that support both worldwide and regional environmental policies. This involves leveraging DL-based super-resolution techniques and multispectral guidance to advance in global high-resolution biomass estimation.

III. DATA

In this section, we present the resources used to develop and train our proposed model, BiomSHARP. We describe the data sources, preprocessing techniques, and selected regions to facilitate reproducibility. Table I summarizes the details of each experiment.

For our task, we required (i) biomass data with a resolution similar to what will be available from near future satellite missions, (ii) high-resolution biomass data to serve as ground truth

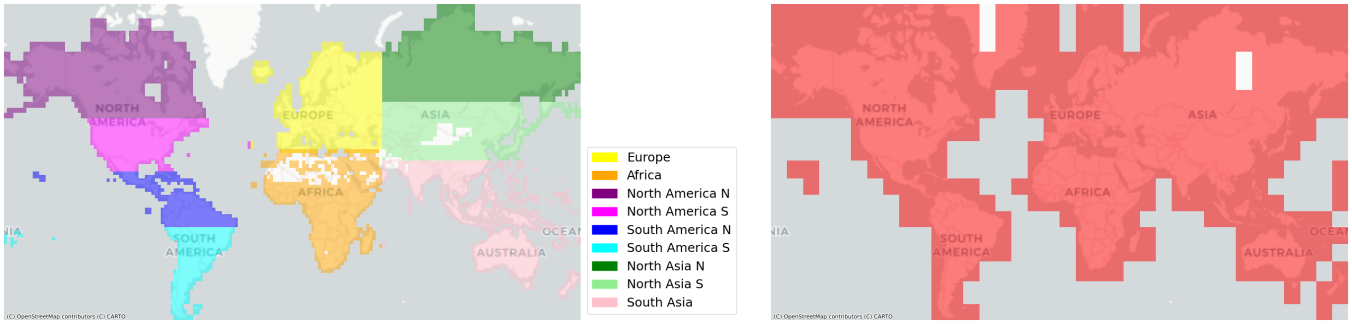

(a) (b)

Fig. 1. Global biomass data. (a) Biomass patches at 25m resolution available from [20]–[28]. (b) Biomass patches at 100m resolution available from [57].

(GT) for training and validation, as well as (iii) high-resolution multispectral images to support resolution enhancement.

To ensure full transparency, all data sources used in this study are publicly accessible, allowing for independent verification and further exploration by the research community.

A. Datasets

In this subsection, we detail the specific datasets used in our study, encompassing high-resolution biomass data serving as ground truth, low-resolution biomass data analogous to future satellite mission outputs, and high-resolution multispectral imagery guiding in resolution enhancement. Below, we describe each dataset, highlighting its features, sources, and role in our methodology.

1) High-resolution biomass: For the high-resolution biomass data, we used two different datasets, depending on the particular experiment. First, we used the "GlobBiomass dataset of forest biomass (25 m)", which is publicly available on Zenodo and divided into 9 regions: Eurasia [20], Africa [21], North America N [22], North America S [23], South America N [26], South America S [27], North Asia N [24], North Asia S [25], and South Asia [28]. This dataset provides a global map of above-ground forest biomass estimates for the year 2010 at a 25-meter resolution, and was used for the training of all models and the evaluation of the first three experiments. Fig. 1a illustrates the extension of the area covered by this dataset. For the validation of the final experiment, in which we check the generalization of BiomSHARP in the temporal domain, we have used another dataset, FORMS, an AGB map at 30-meter resolution of France from 2020, presented in [58].

2) Low-resolution biomass: For the low-resolution biomass data, since the previously mentioned satellites (NISAR and BIOMASS missions) have not yet been launched, we utilized the "ESA Biomass Climate Change Initiative (Biomass_cci): Global datasets of forest above-ground biomass for the years 2010, 2017, 2018, 2019 and 2020, v4" [57], which offers data at a resolution of 100 meters—the same resolution expected from NASA-ISRO's NISAR mission. Specifically, we used the data from 2010 (to align with the year of the 25m-resolution biomass data) and from 2020 (for the validation of the temporal experiment). Fig. 1b illustrates the extension of the area covered by this dataset.

3) High-resolution multispectral data: In this study, we used multispectral optical data from both Landsat-5 and Sentinel-2 satellites. Sentinel-2 provides images with higher spatial and spectral resolution but was not launched until 2015, which is five years after the 2010 biomass data. In contrast, Landsat-5 offers imagery from 1984 to 2013, including the year of the biomass data, 2010, but it has lower spatial and spectral resolution compared to Sentinel-2. Therefore, we experimented with both datasets to determine which approach is more effective for guided biomass super-resolution. Specifically, we aimed to establish whether using guide images that are temporally closer to the biomass data is more advantageous than employing images with higher spatial and spectral resolution acquired at a later time. The data was obtained using Google Earth Engine (GEE) [59]. For Sentinel-2, we utilized the Level-2A product [60] and, for Landsat-5, we selected the Level-2, Collection 2, Tier 1 product [61] . Sentinel-2 offers images with 13 spectral bands, with resolutions ranging from 10 to 60 meters per pixel, depending on the band. For our analysis, we selected the 10 bands with resolutions of 10 or 20 meters, as these provide the detail required for our study. We then downsampled these higher-resolution bands to align them with our target resolution of 25 meters. The Landsat-5 product includes 6 bands at a 30-meter resolution. Therefore, to obtain the objective resolution of 25 meters defined in our study, we applied interpolation to resample the data accordingly. For the State-of-the-Art (SOTA) Comparison and Band Redundancy experiments we used multispectral data from only one year: 2010 for Landsat-5 and 2017 for Sentinel-2 (the first available year in GEE for this product). However, in the Global Generalization experiment, the time span was extended to 2009–2011 for Landsat-5 and to 2017–2019 for Sentinel-2 to include more of the Earth surface. Finally, for the validation of the Temporal Generalization experiment, we only used Sentinel-2 data from 2020. In all cases, we used the median to obtain a single representative image from the collection of images available in the specified period of time.

B. Data preprocessing

For the biomass data (both low and high-resolution), no preprocessing was applied.

For the Sentinel-2 data, we filtered out pixels with clouds using the given classification in band SCL, and computed the

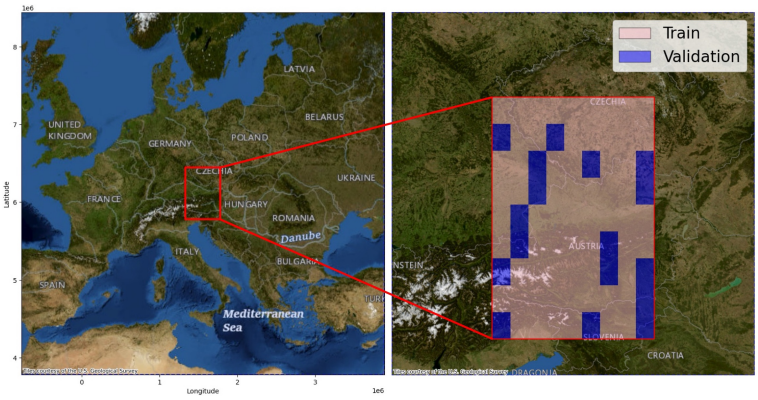

Fig. 2. (Left) Region of Europe showing the AoI of the study, represented by a red box and defined by the bounding box coordinates `[12.0, 46.0, 16.0, 50.0]` in EPSG:4326. (Right) Distribution of the AoI between training and validation sets (see Sections V-A and V-B).

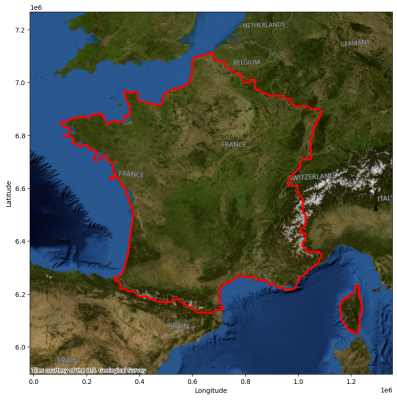

Fig. 3. Region of France (red polygons) used to evaluate the model in the Temporal Generalization experiment (see Section V-D).

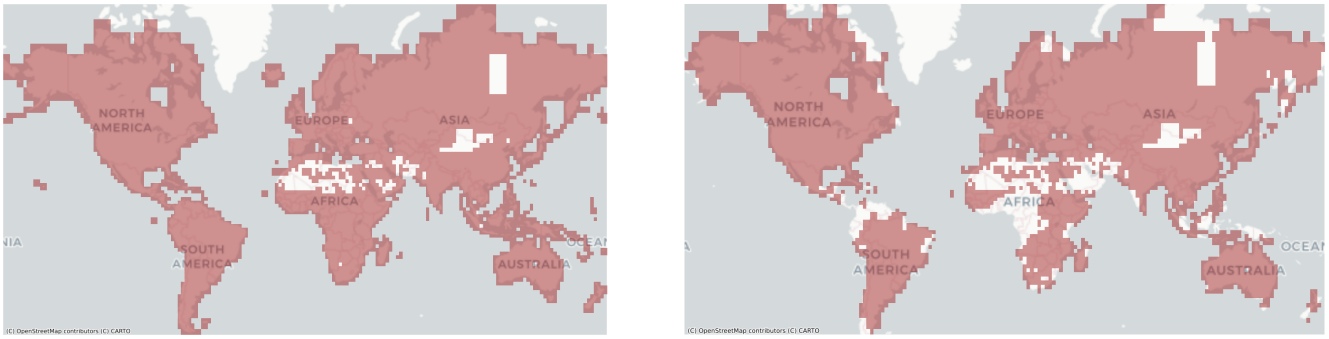

(a) (b)

Fig. 4. Global area studied in the Global Generalization experiment (see Section V-C), derived from intersecting available data across all utilized datasets (biomass at 25 and 100 meters of resolution, and the multispectral images available in GEE). (a) Sentinel-2 as the multispectral data. (b) Landsat-5 as the multispectral data.

median of the remaining pixels to produce a single final image. For the Landsat-5 data, we specified a CLOUD_COVER lower than 15%, and computed the median of the images to produce the final image. The specific JavaScript code used to download and process the Sentinel-2 and Landsat-5 data for the small-scale experiments within the AoI (see Section III-C) can be found in our GitHub repository.

For the GEE data, we reprojected[1] the Sentinel-2 and Landsat-5 images in order to match the 25-meter resolution, projection, and extent of the biomass raster.

C. Region of study

In this study, we have worked with different regions. For the first two experiments, SOTA Comparison and Band Redundancy (in Sections V-A and V-B, respectively), we defined a small area of interest (AoI), illustrated in Fig. 2. This AoI was chosen for its manageable size and computational convenience, allowing for the efficient comparison of different models under controlled but varied environmental conditions.

For the Global Generalization experiment (in Section V-C) we used all global data according to the spatial availability of the three data sources (low and higher AGB data, and multispectral imagery). Fig. 4 illustrates the global region used in this particular experiment.

Finally, for the Temporal Generalization experiment (in Section V-D), we took the model chosen in the Band Redundancy experiment—trained on the AoI—and evaluated it on the FORMS dataset region, which covers France and Corsica (see Fig. 3).

[1]Reprojection was done via the function `rio.reproject_match()` from the `rioxarray` package.

IV. Models

In this section, we present the models evaluated in our study, including our proposed BiomSHARP model and several baseline models adapted for comparison. BiomSHARP is specifically designed to enhance the resolution of AGB rasters by leveraging high-resolution Sentinel-2 or Landsat-5 data. To ensure a fair assessment, all models are standardized in terms of input crop size, training strategy, and parameter count. This allows us to rigorously compare the performance improvements offered by BiomSHARP over existing approaches. Complete hyperparameter details for all models are available in our GitHub repository.

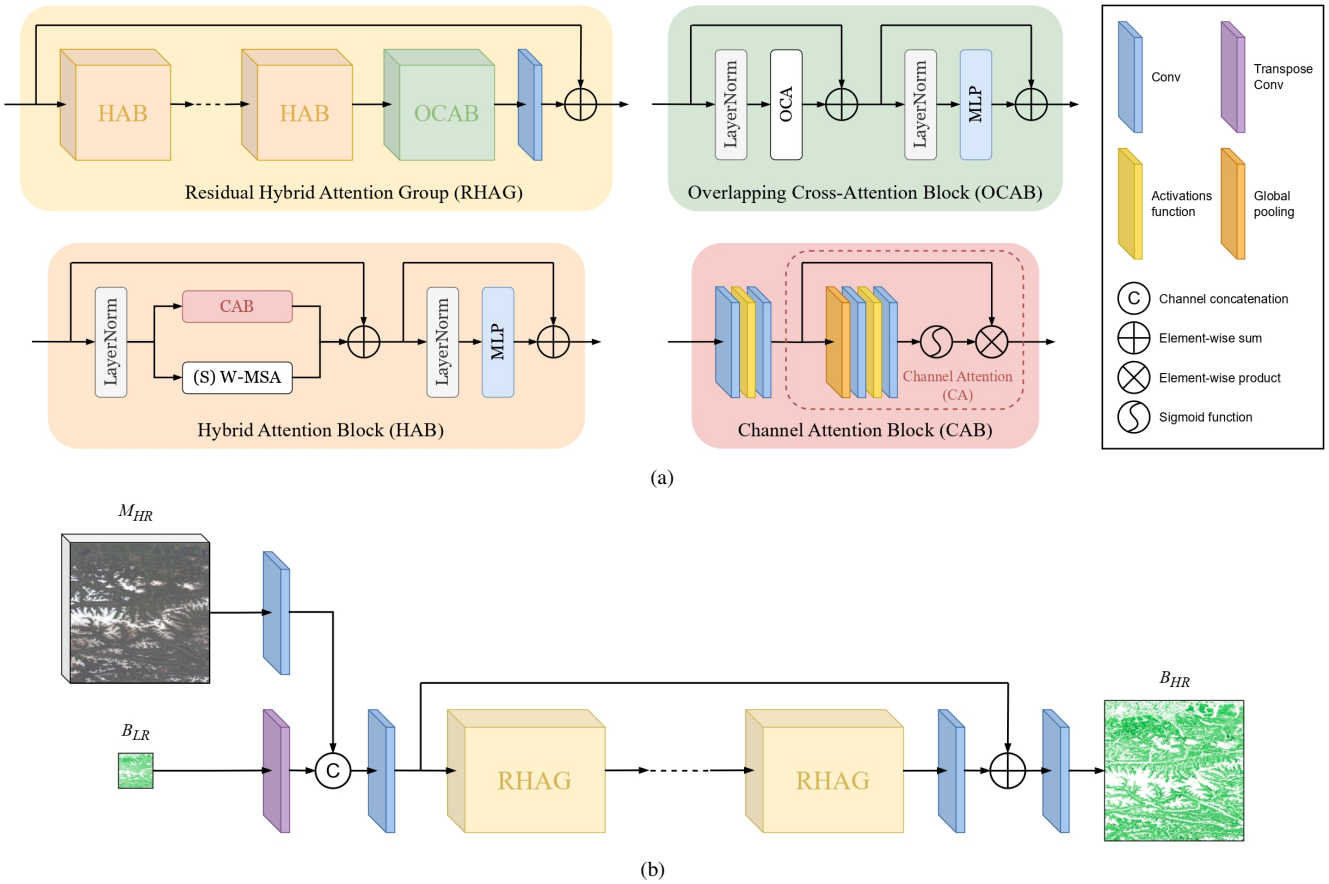

Fig. 5. BiomSHARP architecture, based on the RHAG module from HAT proposed in [41], [42]. (a) Detailed view of individual submodules where each colored box represents a specific submodule. (b) Overall network architecture, with the same color code.

A. Baselines

To ensure comparability among all models, we standardized the ground truth crop size to 256×256 and adopted a unified training strategy—training from scratch with an interpolation factor of 4 in each dimension. Additionally, we adjusted the number of filters or features in some baseline models to ensure that the number of parameters is in the same order of magnitude across all models.

1) ReUse: The ReUse model [8] is the first end-to-end DL model designed to predict AGB from Sentinel-2 data. It is based on a Regressive U-Net [62] and is the only baseline model in this study originally intended for biomass data. The original model has 10 input channels, corresponding to the 10 bands of Sentinel-2. For our experiments with Landsat-5, we modified this number to 6, to match the 6 bands of this satellite. Since ReUse is the only baseline model specifically designed to handle satellite and biomass data, we used it as a reference and adapted all the other baseline models (originally designed to process only natural RGB images) to use all the bands of Sentinel-2 or Landsat-5 as input in order to achieve a fair comparison. Also, in the original paper, crops of size 16×16 were used, with 16 filters, resulting in a model with 1.2 million parameters. For this study, we increased the crop size (from 16 to 256) to use the same size in all models, and we also increased the number of filters (from 16 to 24) to observe the improvement in performance when increasing the capacity of the model, and making it more comparable to the other models. In Tables II and III, the modified model with 24 filters is represented as ReUse*. We also changed the learning rate scheduler (from a `ReduceLROnPlateau` to an `ExponentialDecay`) to enhance training convergence and performance.

2) HAT-S: The HAT model [41], [42] is a state-of-the-art image super-resolution model that utilizes the Residual Hybrid Attention Group (RHAG) module at its core (see Fig. 5a for the detailed structure of this module). RHAG enhances both local and global interactions by integrating channel attention with window-based cross- and self-attention schemes through hybrid attention blocks and overlapping cross-attention mechanisms. By activating a wide range of input pixels and facilitating cross-window interactions, RHAG enables precise reconstruction of fine details. This model has three versions based on parameter count; in this study, we used the smallest version, HAT-S, which comprises 6 RHAG modules (each with 6 HAB modules) and has an embedding dimension of 144, amounting to approximately 9.5 million parameters. By selecting this smaller version of the HAT model, we ensure comparability with the other tested models in terms of parameter count. However, this model was originally designed to improve the resolution of RGB images, so we adapted it for our biomass data (e.g. by changing the number of input channels and modifying the input normalization value).

3) SGNet: The SGNet model [43] is a state-of-the-art guided super-resolution model developed for depth map super-resolution, a task we consider closely related to our problem. This model has not been applied to biomass data before, hence, we adapted it for our study. In particular, we changed the number of channels of the input guide data to match the number of bands used from Sentinel-2 or Landsat-5. Additionally, we reduced the number of filters (from 24 to 16) to achieve a model with 4.2 million parameters in order to assess the performance of the model with a capacity closer to that of the other models. In Tables II and III, the modified model with 16 filters is represented as SGNet*.

B. BiomSHARP

In this study, we introduce BiomSHARP, a DL model designed to enhance the resolution of AGB rasters by an interpolation factor of 4 in each dimension, with the guidance of high-resolution multispectral data. This model, depicted in Fig. 5, builds upon the RHAG module introduced in HAT [41], [42] (yellow box in Fig. 5a and Fig. 5b), originally designed for natural image super-resolution, but here used to perform biomass guided super-resolution, enhancing the resolution of AGB rasters using multispectral images from Sentinel-2 or Landsat-5 as guidance.

In the original HAT model, the input is a low-resolution (LR) RGB image that passes through a convolution layer to preserve its spatial dimensions. The resulting shallow features are then processed by a set of RHAG modules, which also maintains spatial dimensions, and the output is combined with the initial shallow features via a residual connection. The combined features are subsequently upscaled using the Pixel Shuffle method [63] to obtain the final enhanced image.

For BiomSHARP, we have replaced the initial convolution layer with a transpose convolution layer. This not only extracts shallow features from the LR biomass data but also upscales them to the desired spatial resolution at the output. Concurrently, multispectral data (from Sentinel-2 or Landsat-5), matching the target output resolution, is processed through a convolution layer that preserves its spatial dimension. These shallow features from the multispectral data are then concatenated with the upscaled shallow features from the LR biomass data. This concatenation allows the subsequent layers—particularly the attention-based modules—to effectively learn how to merge and exploit the complementary information from both data sources. Afterward, this combined feature set is processed by another convolution layer to integrate the features, which are then passed through five RHAG modules from HAT—each composed of six HAB modules with an embedding dimension of 84 (see Fig. 5a for more details on these modules). The number of RHAG modules was treated as a hyperparameter; we selected five during tuning as a trade-off between strong performance and model complexity, deviating from the original HAT configuration of six modules. Following [41], [42], the deep features obtained pass through a convolution layer and then are added back to the combined shallow features using a residual connection. This residual connection helps preserve low-level information from the shallow features and facilitates gradient flow during training, which is a common practice in deep learning to stabilize and improve convergence. Finally, a convolution layer is used to generate the AGB prediction from the extracted features. By initially upscaling the biomass, we leverage the high-resolution details from the multispectral data more effectively during the concatenation of both feature sets.

V. Experiments: Set Up and Results

In this section, we present four main experiments designed to evaluate BiomSHARP under different conditions. First, in the SOTA Comparison experiment (Section V-A), we compare BiomSHARP against classical and deep learning interpolation methods using several performance metrics to demonstrate its superior reconstruction quality. Second, in the Band Redundancy experiment (Section V-B), we assess whether reducing the number of spectral bands can maintain performance while lowering memory usage. Third, in the Global Generalization experiment (Section V-C), we test the ability of BiomSHARP to generalize worldwide across diverse climatic zones, even when trained on a limited subset of data. Finally, in the Temporal Generalization experiment (Section V-D), we evaluate the model's robustness over time by predicting biomass for a future year and comparing these results with other interpolation methods.

A. State-of-the-Art Comparison

The goal of this experiment is to compare the performance of the proposed BiomSHARP model against a classic interpolation method (bicubic) and three DL approaches: ReUse [8], HAT [41] and SGNet [43]. Among these, only the ReUse model has been tested on biomass data, whereas the last two have not. For consistency, all models, including BiomSHARP, were trained using the L1 loss, except SGNet, which employs a specialized loss combining spatial, gradient, and frequency terms.

Specifically, each model was trained from scratch three times, each with a different random seed to capture initialization variability. In addition, hyperparameter tuning was performed for all models to ensure optimal results.

The region of study for this experiment was the AoI presented in Section III-C, which we divided into 81 patches of size 1920×1920 and randomly allocated 64 for training and 17 for validation (see Fig. 2).

Regarding the multispectral bands, in this experiment we used all of them, 10 in the case of Sentinel-2 and 6 for Landsat-5, in order to compare the methods in the best case scenario (when we have all possible spectral information).

Tables II and III present the results of the experiment, using Sentinel-2 and Landsat-5 bands as guidance, respectively. The experiments evaluate the performance of the proposed method across multiple metrics, including Peak Signal-to-Noise Ratio (PSNR), Structural Similarity Index Measure (SSIM), Mean Squared Error (MSE), Root Mean Squared Error (RMSE), and Mean Absolute Error (MAE). PSNR and SSIM are the most widely used metrics for assessing image super-resolution and reconstruction quality [31], [33], [34], while MSE, RMSE, and

TABLE II
COMPARISON OF MODELS USING 10-20M SENTINEL-2 BANDS. MODELS USE HIGH-RESOLUTION MULTISPECTRAL DATA (MS), LOW-RESOLUTION AGB DATA (AGB), OR BOTH. RESULTS ARE AVERAGED OVER 3 RUNS WITH DIFFERENT RANDOM INITIALIZATIONS AND REPORTED AS "MEAN (STD)". BOLD INDICATES THE BEST RESULT FOR EACH METRIC.

Model	MS	AGB	Params (↓)	PSNR (↑)	SSIM (↑)	MSE (↓)	RMSE (↓)	MAE (↓)
Bicubic		✓	-	17.25 (-)	0.36 (-)	7404.83 (-)	81.68 (-)	56.65 (-)
HAT-S [41], [42]		✓	9.6 M	21.61 (0.02)	0.49 (1.8e-3)	2531.54 (22,97)	48.58 (0.16)	32.11 (0.05)
ReUse [8]	✓		1.2 M	23.07 (0.02)	0.60 (1.4e-3)	1952.91 (13.34)	41.82 (0.11)	27.09 (0.10)
ReUse*	✓		4.9 M	23.20 (0.03)	0.61 (1.6e-3)	1895.39 (16.83)	41.19 (0.17)	26.60 (0.13)
SGNet*	✓	✓	4.2 M	24.13 (0.05)	0.64 (2.3e-3)	1503.42 (13.39)	36.89 (0.19)	23.92 (0.14)
SGNet [43]	✓	✓	9.2 M	24.42 (0.04)	0.66 (1.8e-3)	1400.91 (15.27)	35.64 (0.17)	22.79 (0.14)
BiomSHARP (our)	✓	✓	3.4 M	**24.90** (0.06)	**0.70** (3.1e-3)	**1254.24** (14.60)	**33.70** (0.21)	**21.02** (0.15)

TABLE III
COMPARISON OF MODELS USING ALL MULTISPECTRAL LANDSAT-5 BANDS. MODELS USE HIGH-RESOLUTION MULTISPECTRAL DATA (MS), LOW-RESOLUTION AGB DATA (AGB), OR BOTH. RESULTS ARE AVERAGED OVER 3 RUNS WITH DIFFERENT RANDOM INITIALIZATIONS AND REPORTED AS "MEAN (STD)". BOLD INDICATES THE BEST RESULT FOR EACH METRIC.

Model	MS	AGB	Params (↓)	PSNR (↑)	SSIM (↑)	MSE (↓)	RMSE (↓)	MAE (↓)
Bicubic		✓	-	17.25 (-)	0.36 (-)	7404.83 (-)	81.68 (-)	56.65 (-)
HAT-S [41], [42]		✓	9.6 M	21.61 (0.02)	0.49 (1.8e-3)	2531.54 (22,97)	48.58 (0.16)	32.11 (0.05)
ReUse [8]	✓		1.2 M	23.44 (0.02)	0.62 (2.8e-3)	1820.05 (12.83)	40.24 (0.12)	26.27 (0.10)
ReUse*	✓		4.9 M	23.60 (0.04)	0.63 (7.6e-4)	1755.12 (10.40)	39.50 (0.15)	25.70 (0.08)
SGNet*	✓	✓	4.2 M	24.56 (0.02)	0.67 (3.5e-4)	1360.05 (6.39)	35.08 (0.08)	22.63 (0.03)
SGNet [43]	✓	✓	9.2 M	24.80 (0.01)	0.69 (3.5e-4)	1280.10 (1.48)	34.09 (0.02)	21.68 (0.04)
BiomSHARP (our)	✓	✓	3.4 M	**25.14** (0.02)	**0.71** (1.4e-3)	**1194.81** (7.95)	**32.84** (0.10)	**20.45** (0.06)

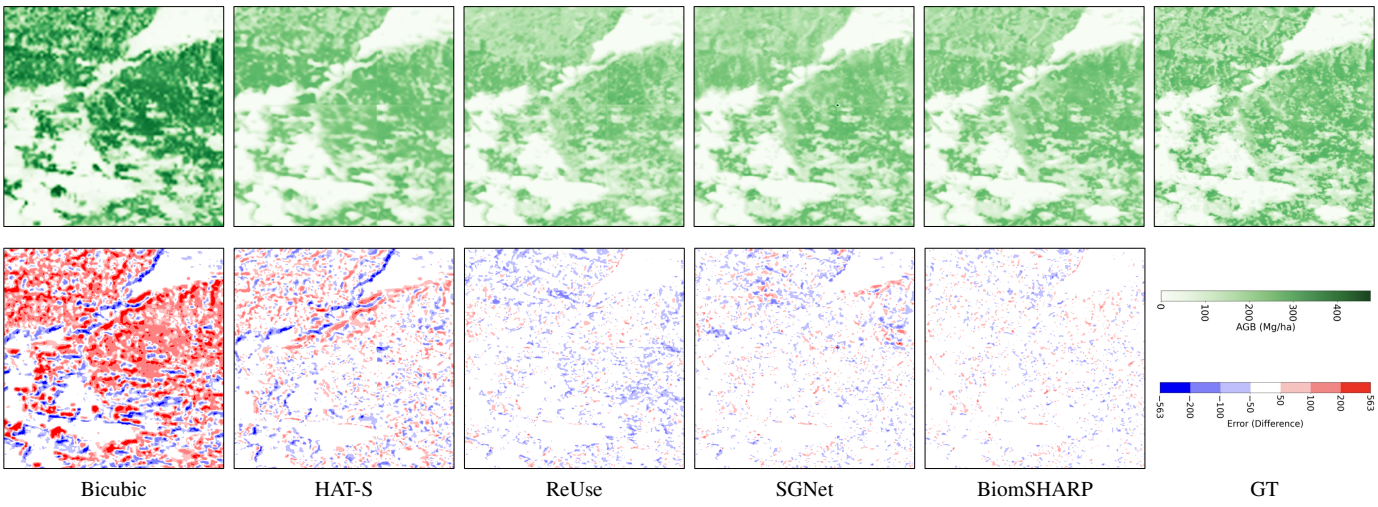

Fig. 6. Qualitative results for Landsat-5 (similar results were obtained with Sentinel-2). (Top) Predicted AGB maps. (Bottom) Error maps relative to the GT. Note the lower error values in BiomSHARP, even compared to SGNet.

MAE are commonly applied for evaluating continuous value prediction in regression tasks [64], [65]. Higher values indicate better performance for PSNR and SSIM, whereas lower values of MSE, RMSE and MAE reflect smaller prediction errors.

Results show that BiomSHARP consistently outperforms all other methods across every metric in both Sentinel-2 and Landsat-5 experiments, highlighting its ability to produce high-quality biomass reconstructions. Integrating low-resolution AGB data ('AGB') with high-resolution multispectral data ('MS') offers clear benefits over relying on a single data type. This is exemplified by the superior performance of SGNet and BiomSHARP, with BiomSHARP surpassing SGNet, even though it has nearly three times fewer parameters.

When comparing the use of Sentinel-2 (Table II) and Landsat-5 (Table III) as guidance, Landsat-5 consistently achieves slightly better results across all models and metrics.

TABLE IV
GROUPING OF THE DIFFERENT SENTINEL-2 AND LANDSAT-5 BANDS USED IN THIS STUDY AND THEIR CHARACTERISTICS FOR VEGETATION MONITORING, BASED ON [66]–[68]. ONLY SENTINEL-2 BANDS WITH 10 OR 20 METERS OF RESOLUTION ARE USED, AS OUR TARGET RESOLUTION IS 25 METERS.

Sentinel-2 Bands	Landsat-5 Bands	Grouping	Characteristics for vegetation monitoring
B2, B3, B4	B1, B2, B3	Visible bands (VIS)	Chlorophyll in green leaves strongly absorbs light in the visible spectrum, particularly in the blue and red wavelengths, with red being the most absorbed.
B5, B6, B7	–	Red-Edge bands (RE)	RE bands help distinguish photosynthetic activity from biomass and are key indicators for plant health and pigmentation, making them useful for vegetation classification.
B8, B8A	B4	Near-Infrared bands (NIR)	Leaves exhibit high reflectance and transmission in NIR bands, mainly related to leaf structural properties and biomass. B8 (in Sentinel-2) and B4 (in Landsat-5) are particularly useful for shoreline mapping, biomass, and vegetation analysis.
B11, B12	B5, B7	Short-Wave Infrared bands (SWIR)	SWIR bands are mainly absorbed by water, making them useful for measuring soil and vegetation moisture, distinguishing vegetation types and health stress, and differentiating snow from clouds.

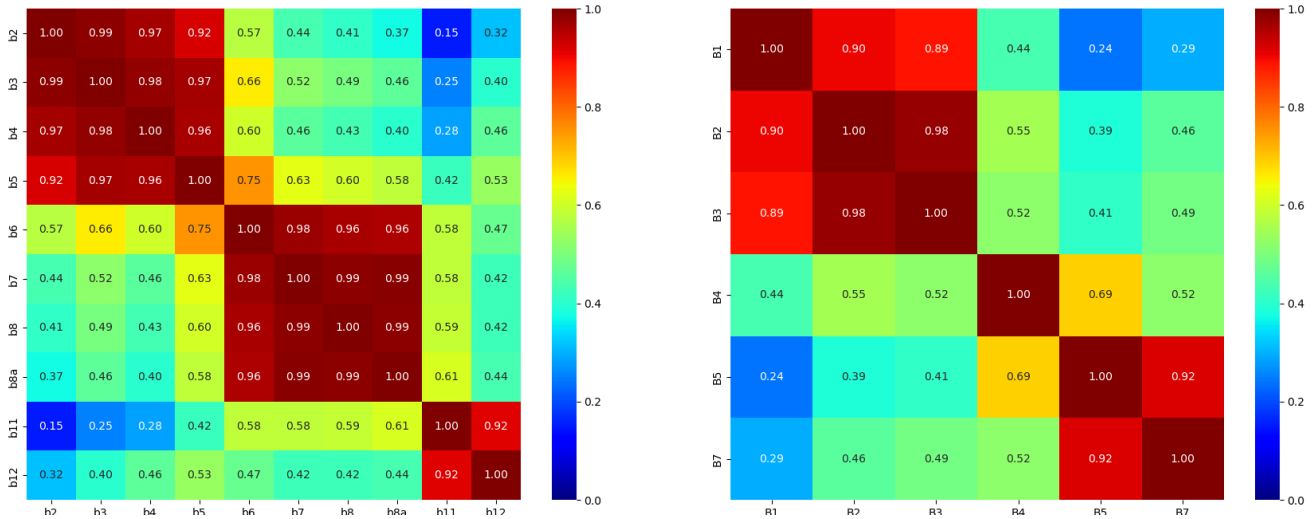

(a) (b)

Fig. 7. Correlation matrix in the AoI for: (a) Sentinel-2 bands. (b) Landsat-5 bands.

This outcome indicates that having multispectral data closer in time to the biomass observations (as with Landsat-5, where both are from 2010) is more beneficial than relying on higher spectral and spatial resolution but recorded further in time (as with Sentinel-2, where biomass data is from 2010 and multispectral data is from 2017). Therefore, the upcoming experiments will primarily focus on Landsat-5 due to its temporal proximity to the biomass observations. Nevertheless, we will continue to conduct general experiments with Sentinel-2, as it is expected to be the satellite of choice in the future—once BIOMASS or NISAR data become available—given its open access and superior spatial, spectral, and temporal resolutions compared to Landsat.

As illustrated by the qualitative results in Fig. 6, BiomSHARP consistently delivers sharper, more detailed predictions that align closer with the ground truth. In the bottom row, the error maps reveal fewer red (blue) patches in BiomSHARP's output, indicating reduced overestimation (underestimation) compared to other methods. Overall, BiomSHARP better preserves critical details—such as boundaries and texture—resulting in cleaner transitions and less blurring. While the enhancements may initially seem subtle, they are consistently present across the scenes, underlining BiomSHARP's superiority in qualitative performance.

B. Band Redundancy

Multispectral bands capture different wavelength ranges, each suited to specific applications. As shown in Table IV, Sentinel-2 and Landsat-5 bands can be grouped into Visible (VIS), Red-Edge (RE), Near-Infrared (NIR), and Short-Wave Infrared (SWIR) categories, each providing distinct benefits for vegetation monitoring.

Until now, we used all available bands to ensure a fair comparison among models. However, the correlation matrices in Fig. 7 reveal strong inter-correlation among certain bands (in both Sentinel-2 and Landsat-5), especially within the same spectral group. Leveraging this redundancy can reduce memory usage without impacting performance. Although prior research [68]–[79] suggests that some bands may be more informative than others for AGB estimation, there is no

TABLE V
COMPARISON OF THE USE OF DIFFERENT LANDSAT-5 BANDS IN BIOMSHARP ON VARIOUS METRICS, TRAINED AND EVALUATED IN THE AOI. THE "MEM." COLUMN REPRESENTS THE MEMORY THAT THE TRAINING DATA OCCUPY IN DISK. WE ALSO INCLUDE THE SGNET MODEL [43] TRAINED WITH ALL BANDS FOR COMPARISON.

Model	Bands	Mem. (↓)	PSNR (↑)	SSIM (↑)	MSE (↓)	RMSE (↓)	MAE (↓)
BiomSHARP	B04	1.8 GB	23.80 (-)	0.62 (-)	1617.37 (-)	38.24 (-)	24.81 (-)
BiomSHARP	B04, B05	3.4 GB	24.53 (-)	0.67 (-)	1365.19 (-)	35.15 (-)	22.32 (-)
BiomSHARP	B04, B07	3.4 GB	24.56 (-)	0.67 (-)	1358.71 (-)	35.07 (-)	22.53 (-)
BiomSHARP	B03, B04	3.4 GB	24.65 (-)	0.68 (-)	1352.54 (-)	34.86 (-)	22.04 (-)
BiomSHARP	B03, B04, B05	5.1 GB	24.86 (-)	0.69 (-)	1284.00 (-)	33.99 (-)	21.40 (-)
BiomSHARP	B03, B04, B07	5.1 GB	24.98 (0.04)	0.70 (1.9e-3)	1238.32 (12.02)	33.44 (0.16)	20.98 (0.08)
BiomSHARP	B01-05, B07 (all)	11 GB	25.14 (0.02)	0.71 (1.4e-3)	1194.81 (7.95)	32.84 (0.10)	20.45 (0.06)
SGNet [43]	B01-05, B07 (all)	11 GB	24.80 (0.01)	0.69 (3.5e-4)	1280.10 (1.48)	34.09 (0.02)	21.68 (0.04)

TABLE VI
COMPARISON OF THE USE OF DIFFERENT SENTINEL-2 BANDS IN BIOMSHARP ON VARIOUS METRICS, TRAINED AND EVALUATED IN THE AOI. IN THE "ALL" BANDS EXPERIMENT, WE ARE USING ALL THE BANDS WITH A RESOLUTION OF 10 OR 20 METERS (WE HAVE EXCLUDED THE 60M-RESOLUTION BANDS SINCE THE OBJECTIVE RESOLUTION IS 25 METERS). THE "MEM." COLUMN REPRESENTS THE MEMORY THAT THE TRAINING DATA OCCUPY IN DISK. WE ALSO INCLUDE THE SGNET MODEL [43] TRAINED WITH ALL BANDS FOR COMPARISON.

Models	Bands	Mem. (↓)	PSNR (↑)	SSIM (↑)	MSE (↓)	RMSE (↓)	MAE (↓)
BiomSHARP	B04, B08, B12	5.1 GB	24.70 (0.02)	0.68 (1.3e-3)	1317.05 (10.56)	34.52 (0.10)	21.70 (0.09)
BiomSHARP	B02-08, B11-12, B8A (all)	17 GB	24.90 (0.06)	0.70 (3.1e-3)	1254.24 (14.60)	33.70 (0.21)	21.02 (0.15)
SGNet [43]	B02-08, B11-12, B8A (all)	17 GB	24.42 (0.04)	0.66 (1.8e-3)	1400.91 (15.27)	35.64 (0.17)	22.79 (0.14)

universally agreed-upon subset or combination of bands for optimal results. Hence, the objective of this experiment is to verify whether fewer bands can preserve performance while reducing memory usage.

To examine these redundancies more closely, we conducted a series of Landsat-5 experiments with different band combinations to identify the most informative sets for biomass estimation. We started with only the NIR band (band 4), known for its sensitivity to leaf structure and high inter-species variability. Next, we added a SWIR band (band 5 or 7) to this NIR setup to capture water content and vegetation stress. Afterward, we introduced a visible band (band 3) alongside the NIR band to incorporate foliar pigment information. Finally, we combined the NIR band with one SWIR band and one visible band to check whether including all three spectral groups yielded a meaningful performance boost over narrower subsets. Given the computational demands, we limited these experiments to Landsat-5 and replicated only the best-performing combination for Sentinel-2.

BiomSHARP consistently shows minimal variability during training (see Tables II and III, with standard deviations below 0.9% of the reported means); therefore, multiple trials for each new experiment were deemed unnecessary. Repeating them would not only use substantial computational resources but also increase the environmental footprint without offering additional insights. Nevertheless, for the sake of completeness, we performed three independent runs for the best-performing band configuration.

The region of study for this experiment was again the AoI presented in Section III-C, with the same train-validation split explained in Section V-A.

The results of the reduced-band experiment are presented in Tables V and VI. Notably, the best-performing configuration—comprising NIR, SWIR (specifically Band 7), and a visible band (Band 3)—achieves performance comparable to using all available bands (next-to-last row in the tables), while requiring less than half the memory. Furthermore, even with only three input bands, BiomSHARP outperforms SGNet (last row in the tables)—the strongest state-of-the-art model evaluated—despite SGNet using the full set of spectral bands and having three times more parameters (see Tables II and III for model sizes).

C. Global Generalization

While the previous experiments focused on a relatively small region in Europe, this section aims to demonstrate BiomSHARP's ability to generalize worldwide with only modest amount of training data. Specifically, we leverage the climate classification from [80] to categorize our data patches into five distinct climatic classes: arid, boreal, equatorial, polar, and warm temperate. After randomly selecting a subset of patches from each class, we train five climate-specific models (one per class) and one global model that aggregates patches from all classes; these models use only the three best-performing bands identified in our Band Redundancy experiment (see Section V-B). For Sentinel-2, we trained only climate-specific models—not a global one—as these models were simpler to optimize and, based on the results with Landsat-5 data, generally outperformed the global model in each climatic region or showed only marginal differences. Fig. 8 illustrates the geographical distribution of the available

data for both Landsat-5 and Sentinel-2, with the climatic classification along with the chosen training patches.

To evaluate the performance of these models across different climates, we report MAE values for each region in Figures 9 and 10, using Landsat-5 and Sentinel-2 as multispectral input data, respectively. As shown, BiomSHARP consistently outperforms the simple upsampling by quadriplicated pixels (Naïve method) and bicubic interpolation in all climatic regions—whether implemented as climate-specific models or as a global model—with one exception: in the polar region using Landsat-5 data, where the baseline methods achieve lower errors. We attribute this exception to the underrepresentation of these low-vegetation, low-biomass areas in our training data, suggesting that additional training samples could enhance performance in these regions. Furthermore, while climate-specific models generally exhibit lower MAE values than the global model—reflecting their specialization in local conditions—the global model remains highly competitive and, in certain instances, even outperforms the specialized models, highlighting its adaptability across multiple regions.

Comparing model performance across climatic regions, boreal, equatorial, and warm temperate areas show higher MAE values—with the equatorial region having the highest error—while arid and polar regions yield much lower errors. This is expected because arid and polar areas have sparse or no vegetation (mostly sand, rocks, and snow), resulting in nearly zero AGB and easier predictions. In contrast, regions with abundant vegetation composed of diverse species (like boreal, equatorial, and warm temperate areas) have higher and more variable AGB values, making accurate predictions more challenging.

Overall, these experiments demonstrate that the benefits of BiomSHARP observed in the AoI of Europe extend successfully to global applications. Training with just a subset of patches from each climatic class is sufficient for BiomSHARP to capture the key characteristics of different vegetation types and environmental contexts.

All these climate-specific models for both Landsat-5 and Sentinel-2, and the global model for Landsat-5, are available to download from our GitHub repository.

D. Temporal Generalization

To further evaluate the reliability of BiomSHARP in real-world applications, we assess its performance in estimating AGB for France in the year 2020. This experiment provides an opportunity to test BiomSHARP's ability to generalize to future years beyond its training data from 2010. By comparing the AGB predictions of BiomSHARP against reference biomass estimates from [58], we can determine whether the model can effectively capture temporal variations in biomass distribution despite being trained on a single reference year. The validation is performed by resampling our model's 25m-resolution biomass predictions to 30m resolution for direct comparison with the reference data (see Section III-A), ensuring consistency in spatial resolution.

The results in Table VII demonstrate that the BiomSHARP model, trained solely on AGB data from 2010 and Sentinel-2 data from 2017 using bands 4, 8, and 12, outperforms the other tested interpolation methods. With a MAE of 14.13 compared to 16.67 for the Naïve method, 15.45 for bicubic, and 15.18 for SGNet, BiomSHARP effectively captures biomass variations despite being trained on data from a decade earlier. Notably, BiomSHARP delivers these results with only 3.4 million parameters, whereas SGNet employs 9.2 million. This indicates strong temporal generalization capability, but suggests that performance could further improve if more recent data were available.

It is important to note that no analogous experiment was conducted using Landsat-5 data, as the sensor was no longer operational in 2020. However, this is not necessary for validating temporal generalization, since the current experiment with Sentinel-2 already demonstrates the capability of BiomSHARP to generalize to future years using only past training data.

TABLE VII
PERFORMANCE COMPARISON OF BIOMSHARP VS. BASELINE MODELS FOR AGB ESTIMATION IN FRANCE (2020). SGNET AND BIOMSHARP WERE TRAINED ON THE AOI (SEE FIG. 2) USING 2010 AGB DATA AS WELL AS 2017 SENTINEL-2 BANDS 4, 8, AND 12.

Model	PSNR (↑)	SSIM (↑)	MSE (↓)	RMSE (↓)	MAE (↓)
Naïve	25.72	0.71	1930.67	39.49	16.67
Bicubic	26.39	0.74	1668.42	36.67	15.45
SGNet [43]	27.04	0.76	1439.41	34.07	15.18
BiomSHARP	**27.47**	**0.78**	**1302.14**	**32.34**	**14.13**

VI. CONCLUSIONS

BiomSHARP leverages guided super-resolution to enhance low-resolution biomass maps by fusing them with high-resolution multispectral data. Our experiments in a predefined AoI demonstrate that BiomSHARP consistently outperforms classic interpolation methods and state-of-the-art DL models across all metrics (MAE, MSE, RMSE, PSNR, and SSIM), while using fewer parameters. This underscores the strength of integrating coarse biomass data with detailed multispectral guidance.

Our analysis comparing Sentinel-2 and Landsat-5 inputs revealed that multispectral data temporally closer to the biomass observations (as with Landsat-5) offers slightly better performance than data with higher spectral and spatial resolution but acquired at a later time (as with Sentinel-2). However, once the BIOMASS and NISAR satellites are launched, biomass observations will be available for the same year as Sentinel-2 data, eliminating the need to sacrifice temporal proximity, spectral detail, or spatial resolution.

Furthermore, our experiments on spectral band redundancy show that even a minimal set of three bands—one NIR, one SWIR, and one VIS—can yield near-optimal results. This reduces memory usage without compromising accuracy. Notably, BiomSHARP with just these three bands still outperforms SGNet, despite SGNet using all bands and having three times more parameters. Global experiments confirmed the robust generalization of the model across almost all climatic regions with both Landsat-5 and Sentinel-2.

Importantly, the temporal generalization experiment for AGB estimation in France 2020 shows that even when trained

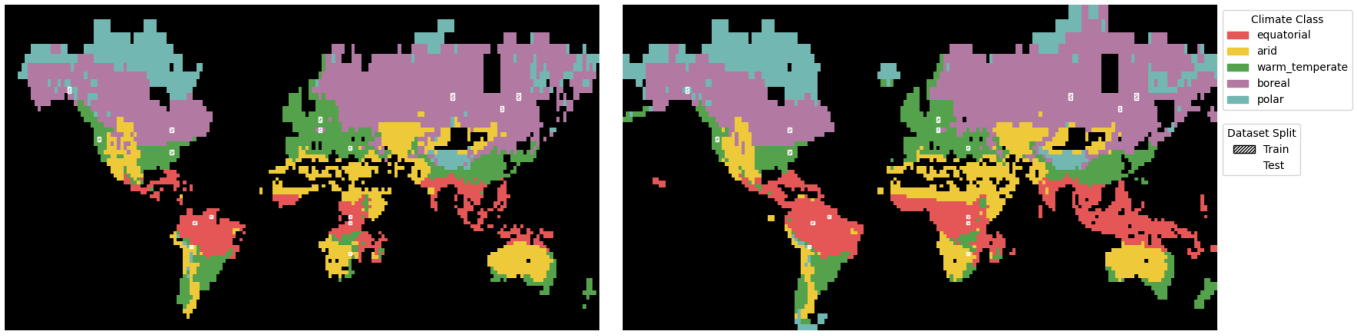

(a) (b)

Fig. 8. Climatic classification of all available patches along with the selected training patches: 4 equatorial, 4 boreal, 4 warm temperate, 2 polar, and 2 arid (only 1 for Landsat-5). Patches with a striped pattern denote the training set, while the remaining patches form the test set. (a) Landsat-5 classification data. (b) Sentinel-2 classification data.

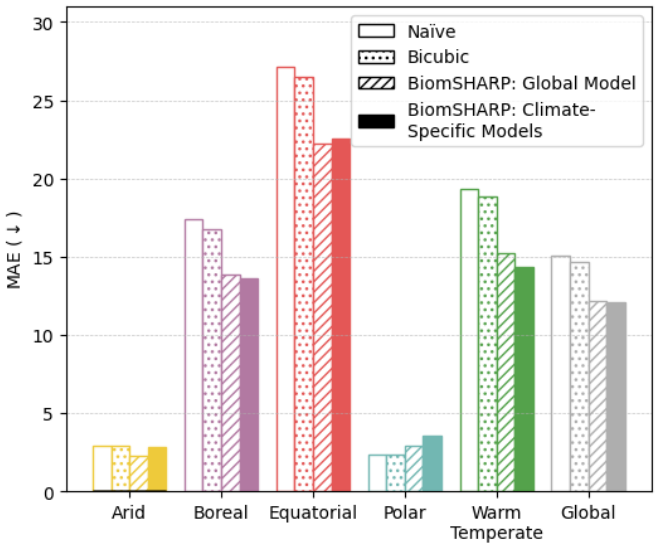

Fig. 9. MAE comparison across climate regions using Landsat-5 multispectral data. Empty bars represent the Naïve method, dotted bars the bicubic method, striped bars BiomSHARP Global Models, and solid bars BiomSHARP Climate-Specific Models.

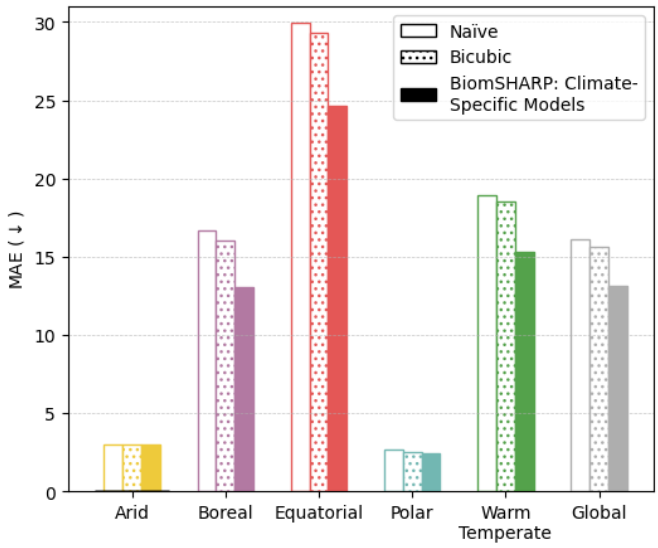

Fig. 10. MAE comparison across climate regions using Sentinel-2 multispectral data. Empty bars represent the Naïve method, dotted bars the bicubic method, and solid bars BiomSHARP Climate-Specific Models.

solely on 2010 data, BiomSHARP not only enhances the resolution of 2020 AGB data but also achieves lower error values compared to other interpolation methods. However, the fact that we only had access to global high-resolution AGB data from 2010 also limits our study; with more recent high-resolution AGB data, we could further improve the model and achieve even better temporal generalization. This suggests that retraining with updated data when available could yield further improvements.

In the near future, as ESA's BIOMASS and NASA-ISRO's NISAR satellites are launched and actual satellite observations becomes available, it will be possible to fine-tune and validate our models to adapt optimally to these new data. To facilitate this, we have released all trained checkpoints—including the global model for Landsat-5 and all climate-specific models for both Landsat-5 and Sentinel-2—in our public GitHub repository, enabling practitioners to apply or adapt BiomSHARP directly to their own regions or datasets.

In conclusion, BiomSHARP offers a promising solution for producing high-resolution biomass maps from low-resolution biomass data, such as the one that will be available from the BIOMASS and NISAR missions. These maps are essential for modeling carbon stocks and flows, monitoring forest health, assessing biodiversity, and tracking ecological disturbances [1]. The demonstrated accuracy, computational efficiency, and adaptability of BiomSHARP make it a valuable tool for enhancing biomass assessments and informing climate policies.

ACKNOWLEDGMENT

The authors would like to thank the European Space Agency (ESA), the United States Geological Survey (USGS), and the Copernicus Programme for providing the satellite data essential to this study. This work was supported by a *Formación de Profesorado Universitario* (FPU) fellowship from the Spanish

Ministry of Science, Innovation and Universities (*Ministerio de Ciencia, Innovación y Universidades*).

REFERENCES

[1] L. Kumar and O. Mutanga, "Remote sensing of above-ground biomass," *Remote Sensing*, vol. 9, no. 9, 2017. doi: 10.3390/rs9090935

[2] European Space Agency, "Biomass Satellite Mission Description," https://earth.esa.int/eogateway/missions/biomass/description, accessed: 29 November 2024.

[3] NASA Jet Propulsion Laboratory, "NASA-ISRO SAR Mission (NISAR) Science Users' Handbook," NASA Jet Propulsion Laboratory, Tech. Rep., august 2019. [Online]. Available: https://nisar.jpl.nasa.gov/system/documents/files/26_NISAR_FINAL_9-6-19.pdf

[4] P. Wai, H. Su, and M. Li, "Estimating aboveground biomass of two different forest types in myanmar from sentinel-2 data with machine learning and geostatistical algorithms," *Remote Sensing*, vol. 14, no. 9, p. 2146, 2022.

[5] L. L. Narine, S. C. Popescu, and L. Malambo, "Synergy of icesat-2 and landsat for mapping forest aboveground biomass with deep learning," *Remote Sensing*, vol. 11, no. 12, 2019. doi: 10.3390/rs11121503

[6] A. T. N. Dang, S. Nandy, R. Srinet, N. V. Luong, S. Ghosh, and A. S. Kumar, "Forest aboveground biomass estimation using machine learning regression algorithm in yok don national park, vietnam," *Ecological Informatics*, vol. 50, pp. 24–32, 2019.

[7] X. Tian, J. Li, F. Zhang, H. Zhang, and M. Jiang, "Forest aboveground biomass estimation using multisource remote sensing data and deep learning algorithms: A case study over hangzhou area in china," *Remote Sensing*, vol. 16, no. 6, 2024. doi: 10.3390/rs16061074

[8] A. E. Pascarella, G. Giacco, M. Rigiroli, S. Marrone, and C. Sansone, "Reuse: Regressive unet for carbon storage and above-ground biomass estimation," *Journal of Imaging*, vol. 9, no. 3, 2023. doi: 10.3390/jimaging9030061

[9] L. V. Schreiber, J. G. A. Amorim, L. Guimarães, D. M. Matos, C. M. da Costa, and A. Parraga, "Above-ground biomass wheat estimation: Deep learning with uav-based rgb images," *Applied Artificial Intelligence*, vol. 36, no. 1, p. 2055392, 2022. doi: 10.1080/08839514.2022.2055392

[10] S. Ghosh and M. Behera, "Aboveground biomass estimates of tropical mangrove forest using sentinel-1 sar coherence data - the superiority of deep learning over a semi-empirical model," *Computers & Geosciences*, vol. 150, p. 104737, 2021. doi: 10.1016/j.cageo.2021.104737

[11] T. K. Ho, "Random decision forests," in *Proceedings of 3rd International Conference on Document Analysis and Recognition*, vol. 1, 1995, pp. 278–282 vol.1. doi: 10.1109/ICDAR.1995.598994

[12] Y. LeCun, Y. Bengio, and G. Hinton, "Deep learning," *Nature*, vol. 521, no. 7553, pp. 436–444, May 2015. doi: 10.1038/nature14539

[13] R. Yang, S. K. Singh, M. Tavakkoli, N. Amiri, Y. Yang, M. A. Karami, and R. Rai, "Cnn-lstm deep learning architecture for computer vision-based modal frequency detection," *Mechanical Systems and Signal Processing*, vol. 144, p. 106885, 2020. doi: 10.1016/j.ymssp.2020.106885

[14] A. Baccini, S. Goetz, W. Walker, N. Laporte, M. Sun, D. Sulla-Menashe, J. Hackler, P. Beck, R. Dubayah, M. Friedl, S. Samanta, and R. Houghton, "Estimated carbon dioxide emissions from tropical deforestation improved by carbon-density maps," *Nature Clim. Change*, vol. 2, pp. 182–185, doi:10.1038/nclimate1354, 01 2012. doi: 10.1038/nclimate1354

[15] S. Saatchi, N. Harris, S. Brown, M. Lefsky, E. Mitchard, W. Salas, B. Zutta, W. Buermann, S. Lewis, S. Hagen, S. Petrova, L. White, M. Silman, and A. Morel, "Benchmark map of forest carbon stocks in tropical regions across three continents," *Proceedings of the National Academy of Sciences of the United States of America*, vol. 108, pp. 9899–904, 06 2011. doi: 10.1073/pnas.1019576108

[16] C. Neigh, R. Nelson, K. Ranson, H. Margolis, P. Montesano, G. Sun, V. Kharuk, E. Næsset, M. Wulder, and H.-E. Andersen, "Taking stock of circumboreal forest carbon with ground measurements, airborne and spaceborne lidar," *Remote Sensing of Environement*, vol. 137, pp. 274–287, 10 2013. doi: 10.1016/j.rse.2013.06.019

[17] D. J. Zarin, N. L. Harris, A. Baccini, D. Aksenov, M. C. Hansen, C. Azevedo-Ramos, T. Azevedo, B. A. Margono, A. C. Alencar, C. Gabris, A. Allegretti, P. Potapov, M. Farina, W. S. Walker, V. S. Shevade, T. V. Loboda, S. Turubanova, and A. Tyukavina, "Can carbon emissions from tropical deforestation drop by 50% in 5 years?" *Global Change Biology*, vol. 22, no. 4, pp. 1336–1347, 2016. doi: 10.1111/gcb.13153

[18] M. Simard, L. Fatoyinbo, C. Smetanka, V. H. Rivera-Monroy, E. Castañeda-Moya, N. Thomas, and T. Van der Stocken, "Mangrove canopy height globally related to precipitation, temperature and cyclone frequency," *Nature Geoscience*, vol. 12, no. 1, pp. 40–45, Jan 2019. doi: 10.1038/s41561-018-0279-1

[19] N. Harris, D. Gibbs, A. Baccini, R. Birdsey, S. de Bruin, M. Farina, L. Fatoyinbo, M. Hansen, M. Herold, R. Houghton, P. Potapov, D. Requena Suarez, R. M. Roman-Cuesta, S. Saatchi, C. Slay, S. Turubanova, and A. Tyukavina, "Global maps of twenty-first century forest carbon fluxes," *Nature Climate Change*, vol. 11, pp. 1–7, 03 2021. doi: 10.1038/s41558-020-00976-6

[20] M. Santoro and O. Cartus, "GlobBiomass dataset of forest biomass, Eurasia (25 m)," Jan. 2023. doi: 10.5281/zenodo.7540824

[21] ——, "GlobBiomass dataset of forest biomass, Africa (25 m)," Apr. 2021. doi: 10.5281/zenodo.4725667

[22] ——, "GlobBiomass dataset of forest biomass, North America N (25 m)," Jan. 2023. doi: 10.5281/zenodo.7550809

[23] ——, "GlobBiomass dataset of forest biomass, North America S (25 m)," Jan. 2023. doi: 10.5281/zenodo.7550246

[24] ——, "GlobBiomass dataset of forest biomass, North Asia N (25 m)," Jan. 2023. doi: 10.5281/zenodo.7584224

[25] ——, "GlobBiomass dataset of forest biomass, North Asia S (25 m)," Jan. 2023. doi: 10.5281/zenodo.7584753

[26] ——, "GlobBiomass dataset of forest biomass, South America N (25 m)," Jan. 2023. doi: 10.5281/zenodo.7544238

[27] ——, "GlobBiomass dataset of forest biomass, South America S (25 m)," Sep. 2023. doi: 10.5281/zenodo.8334607

[28] ——, "GlobBiomass dataset of forest biomass, South Asia (25 m)," Jan. 2023. doi: 10.5281/zenodo.7545054

[29] L. Yue, H. Shen, J. Li, Q. Yuan, H. Zhang, and L. Zhang, "Image super-resolution: The techniques, applications, and future," *Signal Processing*, vol. 128, pp. 389–408, 2016. doi: 10.1016/j.sigpro.2016.05.002

[30] X. Li and M. Orchard, "New edge-directed interpolation," *IEEE Transactions on Image Processing*, vol. 10, no. 10, pp. 1521–1527, 2001. doi: 10.1109/83.951537

[31] H. Chen, X. He, L. Qing, Y. Wu, C. Ren, R. E. Sheriff, and C. Zhu, "Real-world single image super-resolution: A brief review," *Information Fusion*, vol. 79, pp. 124–145, 2022. doi: 10.1016/j.inffus.2021.09.005

[32] C. Dong, C. C. Loy, K. He, and X. Tang, "Learning a deep convolutional network for image super-resolution," in *Computer Vision – ECCV 2014*, D. Fleet, T. Pajdla, B. Schiele, and T. Tuytelaars, Eds. Cham: Springer International Publishing, 2014, pp. 184–199.

[33] L. Salgueiro, J. Marcello, and V. Vilaplana, "Single-image super-resolution of sentinel-2 low resolution bands with residual dense convolutional neural networks," *Remote Sensing*, vol. 13, no. 24, 2021. doi: 10.3390/rs13245007

[34] S. Abadal, L. Salgueiro, J. Marcello, and V. Vilaplana, "A dual network for super-resolution and semantic segmentation of sentinel-2 imagery," *Remote Sensing*, vol. 13, no. 22, 2021. doi: 10.3390/rs13224547

[35] B. Lim, S. Son, H. Kim, S. Nah, and K. M. Lee, "Enhanced deep residual networks for single image super-resolution," in *2017 IEEE Conference on Computer Vision and Pattern Recognition Workshops (CVPRW)*, 2017, pp. 1132–1140. doi: 10.1109/CVPRW.2017.151

[36] Y. Zhang, Y. Tian, Y. Kong, B. Zhong, and Y. Fu, "Residual dense network for image super-resolution," in *Proceedings of the IEEE Conference on Computer Vision and Pattern Recognition (CVPR)*, June 2018.

[37] X. Wang, K. Yu, S. Wu, J. Gu, Y. Liu, C. Dong, Y. Qiao, and C. C. Loy, "Esrgan: Enhanced super-resolution generative adversarial networks," in *Computer Vision – ECCV 2018 Workshops*, L. Leal-Taixé and S. Roth, Eds. Cham: Springer International Publishing, 2019, pp. 63–79.

[38] J. Liang, J. Cao, G. Sun, K. Zhang, L. Van Gool, and R. Timofte, "Swinir: Image restoration using swin transformer," in *2021 IEEE/CVF International Conference on Computer Vision Workshops (ICCVW)*, 2021, pp. 1833–1844. doi: 10.1109/ICCVW54120.2021.00210

[39] Y. Mei, Y. Fan, and Y. Zhou, "Image super-resolution with non-local sparse attention," in *2021 IEEE/CVF Conference on Computer Vision and Pattern Recognition (CVPR)*, 2021, pp. 3516–3525. doi: 10.1109/CVPR46437.2021.00352

[40] S. W. Zamir, A. Arora, S. Khan, M. Hayat, F. S. Khan, and M. Yang, "Restormer: Efficient transformer for high-resolution image restoration," in *2022 IEEE/CVF Conference on Computer Vision and Pattern Recognition (CVPR)*, 2022, pp. 5718–5729. doi: 10.1109/CVPR52688.2022.00564

[41] X. Chen, X. Wang, J. Zhou, Y. Qiao, and C. Dong, "Activating more pixels in image super-resolution transformer," in *IEEE/CVF Conference on Computer Vision and Pattern Recognition, CVPR 2023, Vancouver,*

BC, Canada, June 17-24, 2023. IEEE, 2023, pp. 22 367–22 377. doi: 10.1109/CVPR52729.2023.02142

[42] X. Chen, X. Wang, W. Zhang, X. Kong, Y. Qiao, J. Zhou, and C. Dong, "HAT: hybrid attention transformer for image restoration," *CoRR*, vol. abs/2309.05239, 2023. doi: 10.48550/ARXIV.2309.05239

[43] Z. Wang, Z. Yan, and J. Yang, "Sgnet: Structure guided network via gradient-frequency awareness for depth map super-resolution," in *Thirty-Eighth AAAI Conference on Artificial Intelligence, AAAI 2024, Thirty-Sixth Conference on Innovative Applications of Artificial Intelligence, IAAI 2024, Fourteenth Symposium on Educational Advances in Artificial Intelligence, EAAI 2014, February 20-27, 2024, Vancouver, Canada*, M. J. Wooldridge, J. G. Dy, and S. Natarajan, Eds. AAAI Press, 2024, pp. 5823–5831. doi: 10.1609/AAAI.V38I6.28395

[44] R. de Lutio, S. D'Aronco, J. D. Wegner, and K. Schindler, "Guided super-resolution as a learned pixel-to-pixel transformation," *CoRR*, vol. abs/1904.01501, 2019. [Online]. Available: http://arxiv.org/abs/1904.01501

[45] R. Cong, R. Sheng, H. Wu, Y. Guo, Y. Wei, W. Zuo, Y. Zhao, and S. Kwong, "Learning hierarchical color guidance for depth map super-resolution," *IEEE Transactions on Instrumentation and Measurement*, vol. 73, pp. 1–13, 2024. doi: 10.1109/TIM.2024.3381168

[46] Z. Zhong, X. Liu, J. Jiang, D. Zhao, and X. Ji, "Guided depth map super-resolution: A survey," *ACM Computing Surveys*, vol. 55, no. 14s, p. 1–36, Jul. 2023. doi: 10.1145/3584860

[47] P. L. Suárez, D. Carpio, and A. Sappa, "Boosting guided super-resolution performance with synthesized images," in *2023 17th International Conference on Signal-Image Technology & Internet-Based Systems (SITIS)*, 2023, pp. 189–195. doi: 10.1109/SITIS61268.2023.00036

[48] A. Kasliwal, P. Seth, S. Rallabandi, and S. Singhal, "Corefusion: Contrastive regularized fusion for guided thermal super-resolution," in *2023 IEEE/CVF Conference on Computer Vision and Pattern Recognition Workshops (CVPRW)*. IEEE, Jun. 2023. doi: 10.1109/cvprw59228.2023.00057

[49] C. Arnold, P. Jouvet, and L. Seoud, "Swinfusr: an image fusion-inspired model for rgb-guided thermal image super-resolution," in *IEEE/CVF Conference on Computer Vision and Pattern Recognition, CVPR 2024 - Workshops, Seattle, WA, USA, June 17-18, 2024*. IEEE, 2024, pp. 3027–3036. doi: 10.1109/CVPRW63382.2024.00308

[50] T. Zhang, Y. Fu, L. Huang, S. Li, S. You, and C. Yan, "Rgb-guided hyperspectral image super-resolution with deep progressive learning," *CAAI Transactions on Intelligence Technology*, vol. 9, no. 3, pp. 679–694, 2024. doi: 10.1049/cit2.12256

[51] W. Dong, C. Zhou, F. Wu, J. Wu, G. Shi, and X. Li, "Model-guided deep hyperspectral image super-resolution," *IEEE Transactions on Image Processing*, vol. 30, pp. 5754–5768, 2021. doi: 10.1109/TIP.2021.3078058

[52] C. Chen, Y. Wang, N. Zhang, Y. Zhang, and Z. Zhao, "A review of hyperspectral image super-resolution based on deep learning," *Remote Sensing*, vol. 15, no. 11, 2023. doi: 10.3390/rs15112853

[53] S. Fu, M. Hamilton, L. E. Brandt, A. Feldmann, Z. Zhang, and W. T. Freeman, "Featup: A model-agnostic framework for features at any resolution," in *The Twelfth International Conference on Learning Representations, ICLR 2024, Vienna, Austria, May 7-11, 2024*. OpenReview.net, 2024. [Online]. Available: https://openreview.net/forum?id=GkJiNn2QDF

[54] J. Cao, J. Liang, K. Zhang, Y. Li, Y. Zhang, W. Wang, and L. V. Gool, "Reference-based image super-resolution with deformable attention transformer," in *Computer Vision - ECCV 2022 - 17th European Conference, Tel Aviv, Israel, October 23-27, 2022, Proceedings, Part XVIII*, ser. Lecture Notes in Computer Science, S. Avidan, G. J. Brostow, M. Cissé, G. M. Farinella, and T. Hassner, Eds., vol. 13678. Springer, 2022, pp. 325–342. doi: 10.1007/978-3-031-19797-0_19

[55] N. Metzger, R. C. Daudt, and K. Schindler, "Guided depth super-resolution by deep anisotropic diffusion," in *IEEE/CVF Conference on Computer Vision and Pattern Recognition, CVPR 2023, Vancouver, BC, Canada, June 17-24, 2023*. IEEE, 2023, pp. 18 237–18 246. doi: 10.1109/CVPR52729.2023.01749

[56] Y. Shi, H. Cao, B. Xia, R. Zhu, Q. Liao, and W. Yang, "Dsr-diff: Depth map super-resolution with diffusion model," *Pattern Recognition Letters*, vol. 184, pp. 225–231, 2024. doi: 10.1016/j.patrec.2024.06.025

[57] M. Santoro and O. Cartus, "Esa biomass climate change initiative (biomass_cci): Global datasets of forest above-ground biomass for the years 2010, 2017, 2018, 2019 and 2020, v4," 2023. doi: 10.5285/AF60720C1E404A9E9D2C145D2B2EAD4E

[58] M. Schwartz, P. Ciais, A. De Truchis, J. Chave, C. Ottlé, C. Vega, J.-P. Wigneron, M. Nicolas, S. Jouaber, S. Liu, M. Brandt, and I. Fayad, "Forms: Forest multiple source height, wood volume, and biomass maps in france at 10 to 30m resolution based on sentinel-1, sentinel-2, and global ecosystem dynamics investigation (gedi) data with a deep learning approach," *Earth System Science Data*, vol. 15, no. 11, pp. 4927–4945, 2023. doi: 10.5194/essd-15-4927-2023

[59] N. Gorelick, M. Hancher, M. Dixon, S. Ilyushchenko, D. Thau, and R. Moore, "Google earth engine: Planetary-scale geospatial analysis for everyone," *Remote Sensing of Environment*, 2017. doi: 10.1016/j.rse.2017.06.031

[60] European Space Agency (ESA) and European Commission (Copernicus), "Harmonized sentinel-2 msi: Multispectral instrument, level-2a (surface reflectance)," https://developers.google.com/earth-engine/datasets/catalog/COPERNICUS_S2_SR_HARMONIZED, 2022, data harmonized by Google Earth Engine. Sentinel-2 Level-2A data processed using Sen2Cor.

[61] U.S. Geological Survey, "Landsat 5 collection 2 tier 1 level-2 science products," https://developers.google.com/earth-engine/datasets/catalog/LANDSAT_LT05_C02_T1_L2, 2021, dataset courtesy of the U.S. Geological Survey.

[62] O. Ronneberger, P. Fischer, and T. Brox, "U-net: Convolutional networks for biomedical image segmentation," in *Medical Image Computing and Computer-Assisted Intervention - MICCAI 2015 - 18th International Conference Munich, Germany, October 5 - 9, 2015, Proceedings, Part III*, ser. Lecture Notes in Computer Science, N. Navab, J. Hornegger, W. M. W. III, and A. F. Frangi, Eds., vol. 9351. Springer, 2015, pp. 234–241. doi: 10.1007/978-3-319-24574-4_28

[63] W. Shi, J. Caballero, F. Huszár, J. Totz, A. P. Aitken, R. Bishop, D. Rueckert, and Z. Wang, "Real-time single image and video super-resolution using an efficient sub-pixel convolutional neural network," in *2016 IEEE Conference on Computer Vision and Pattern Recognition (CVPR)*, 2016, pp. 1874–1883. doi: 10.1109/CVPR.2016.207

[64] V. Plevris, G. Solorzano, N. P. Bakas, and M. E. A. Ben Seghier, "Investigation of performance metrics in regression analysis and machine learning-based prediction models," in *8th European Congress on Computational Methods in Applied Sciences and Engineering (ECCOMAS Congress 2022)*. European Community on Computational Methods in Applied Sciences, 2022.

[65] P. Wai, H. Su, and M. Li, "Estimating aboveground biomass of two different forest types in myanmar from sentinel-2 data with machine learning and geostatistical algorithms," *Remote Sensing*, vol. 14, no. 9, 2022. doi: 10.3390/rs14092146

[66] S.-H. by Sinergise, "Sentinel-2 Bands — custom-scripts.sentinel-hub.com," https://custom-scripts.sentinel-hub.com/custom-scripts/sentinel-2/bands/, [Accessed 18-09-2024].

[67] J. Segarra, M. L. Buchaillot, J. L. Araus, and S. C. Kefauver, "Remote sensing for precision agriculture: Sentinel-2 improved features and applications," *Agronomy*, vol. 10, no. 5, 2020. doi: 10.3390/agronomy10050641

[68] A. Imran, K. Khan, N. Ali, N. Ahmad, A. Ali, and K. Shah, "Global journal of environmental science and management narrow band based and broadband derived vegetation indices using sentinel-2 imagery to estimate vegetation biomass article info number of references 32 number of figures 5 number og tables 4," *Global Journal of Environmental Science and Management*, vol. V6, pp. 97–108, 01 2020. doi: 10.22034/gjesm.2020.01.08

[69] C. Li, L. Zhou, and W. Xu, "Estimating aboveground biomass using sentinel-2 msi data and ensemble algorithms for grassland in the shengjin lake wetland, china," *Remote Sensing*, vol. 13, no. 8, 2021. doi: 10.3390/rs13081595

[70] Y. Jin, X. Yang, J. Qiu, J. Li, T. Gao, Q. Wu, F. Zhao, H. Ma, H. Yu, and B. Xu, "Remote sensing-based biomass estimation and its spatio-temporal variations in temperate grassland, northern china," *Remote Sensing*, vol. 6, no. 2, pp. 1496–1513, 2014. doi: 10.3390/rs6021496

[71] S. Puliti, J. Breidenbach, J. Schumacher, M. Hauglin, T. Klingenberg, and R. Astrup, "Above-ground biomass change estimation using national forest inventory data with sentinel-2 and landsat," *Remote Sensing of Environment*, vol. 265, p. 112644, 2021. doi: 10.1016/j.rse.2021.112644

[72] Y. Chen, J. Guerschman, Y. Shendryk, D. Henry, and M. Harrison, "Estimating pasture biomass using sentinel-2 imagery and deep learning," *Remote Sensing*, vol. 13, p. 603, 02 2021. doi: 10.3390/rs13040603

[73] J. A. A. Castillo, A. A. Apan, T. N. Maraseni, and S. G. Salmo, "Estimation and mapping of above-ground biomass of mangrove forests and their replacement land uses in the philippines using sentinel imagery," *ISPRS Journal of Photogrammetry and Remote Sensing*, vol. 134, pp. 70–85, 2017. doi: 10.1016/j.isprsjprs.2017.10.016

[74] Askar, N. Nuthammachot, W. Phairuang, P. Wicaksono, and T. Sayektiningsih, "Estimating aboveground biomass on private forest using sentinel-2 imagery," *Journal of Sensors*, vol. 2018, no. 1, p. 6745629, 2018. doi: 10.1155/2018/6745629

[75] A. B. Baloloy, A. C. Blanco, C. G. Candido, R. J. L. Argamosa, J. B. L. C. Dumalag, L. L. C. Dimapilis, and E. C. Paringit, "Estimation of mangrove forest aboveground biomass using multispectral bands, vegetation indices and biophysical variables derived from optical satellite imageries: Rapideye, planetscope and sentinel-2," *ISPRS Annals of the Photogrammetry, Remote Sensing and Spatial Information Sciences*, vol. IV-3, pp. 29–36, 2018. doi: 10.5194/isprs-annals-IV-3-29-2018

[76] F. Moradi, A. A. Darvishsefat, M. R. Pourrahmati, A. Deljouei, and S. A. Borz, "Estimating aboveground biomass in dense hyrcanian forests by the use of sentinel-2 data," *Forests*, vol. 13, no. 1, 2022. doi: 10.3390/f13010104

[77] Y. Jiang, J. Tao, Y. Huang, J. Zhu, L. Tian, and Y. Zhang, "The spatial pattern of grassland aboveground biomass on Xizang Plateau and its climatic controls," *Journal of Plant Ecology*, vol. 8, no. 1, pp. 30–40, 03 2014. doi: 10.1093/jpe/rtu002

[78] L. Tian, X. Wu, Y. Tao, M. Li, C. Qian, L. Liao, and W. Fu, "Review of remote sensing-based methods for forest aboveground biomass estimation: Progress, challenges, and prospects," *Forests*, vol. 14, no. 6, 2023. doi: 10.3390/f14061086

[79] X. Tian, J. Li, F. Zhang, H. Zhang, and M. Jiang, "Forest aboveground biomass estimation using multisource remote sensing data and deep learning algorithms: A case study over hangzhou area in china," *Remote Sensing*, vol. 16, no. 6, 2024. doi: 10.3390/rs16061074

[80] M. Kottek, J. Grieser, C. Beck, B. Rudolf, and F. Rubel, "World map of the köppen-geiger climate classification updated," *Meteorologische Zeitschrift*, vol. 15, no. 3, pp. 259–263, 07 2006. doi: 10.1127/0941-2948/2006/0130

Laia Albors received the B.S. degree in Data Science and Engineering from the Technical University of Catalonia (UPC), Barcelona, Spain, in 2021, and the M.S. degree in Computer Vision from the Universitat Autònoma de Barcelona (UAB), Barcelona, Spain, in 2022. Before starting her Ph.D., she worked as a Junior Research Engineer at the Barcelona Supercomputing Center (BSC) as part of the Emerging Technologies for Artificial Intelligence group. She is currently pursuing the Ph.D. degree in Computer Vision at UPC, supported by the FPU (*Formación del Profesorado Universitario*) scholarship awarded by the Spanish Ministry of Science, Innovation and Universities. Her research interests include ecological analysis, deep learning, and various applications of computer vision.

Javier Marcello received the M.S. degree in electrical engineering from the Technical University of Catalonia (UPC), Barcelona, Spain, in 1993, and the Ph.D. degree from the Universidad de Las Palmas de Gran Canaria (ULPGC), Las Palmas de Gran Canaria, Spain, in 2006. From 1992 to 2000, he was the Head Engineer of the Spanish Aerospace Defense Administration, Instituto Nacional de Técnica Aeroespacial, Canary Space Center, Maspalomas, Gran Canaria, for different programs (Cospas-Sarsat, MINISAT, Helios, and CREPAD). In 1994, he joined the Department of Signal and Communications, ULPGC, where he is Professor with the Telecommunication School, lecturing on the areas of satellite and radio communications, since 2000. His research is carried out at the Institute of Oceanography and Global Change (IOCAG), ULPGC, which includes multisensor remote sensing image processing (image fusion, classification, and segmentation) and the generation of coastal and land products. He has authored more than 140 works in high impact indexed journals and remote sensing conferences. Dr. Marcello has been the Vice-President of the IEEE Geoscience and Remote Sensing Spanish Chapter from 2016 to 2021.

Ferran Marqués received the degree in electrical engineering and the Ph.D. degree from the Technical University of Catalonia (UPC), Barcelona, Spain, in 1988 and 1992, respectively. From April 1989 to June 1990, he was at the Swiss Federal Institute of Technology, Lausanne (EPFL), Switzerland, and in 1991, he was with the Signal and Image Processing Institute, University of Southern California, Los Angeles. He won the Spanish Best Ph.D. Thesis in Electrical Engineering Award in 1992. Since 2003, he is Full Professor at the Signal Theory and Communications Department at UPC, where he is lecturing in the area of digital signal and image processing. In 2011, he was visiting researcher in the Digital Video and Multimedia Lab, Dept. of Electrical Engineering, Columbia University (NY) USA and received the Jaume Vicens Vives distinction of the Generalitat de Catalunya.

He served as President of the European Association for Signal Processing EURASIP (2002–2004). He has been Associate Editor of the IEEE Transactions on Image Processing and Area Editor of the Elsevier journal Signal Processing: Image Communication. He has been Dean of the Telecommunication School at UPC (2012-2019). He is author or co-author of more than 150 publications that have appeared as journal papers and proceeding articles, 2 books, several book chapters and 4 international patents.